Preparation and characterization of a new cobalt hydrazone complex and its catalytic activity in the hydrogenation of carbon monoxide (Fischer–Tropsch synthesis)

Halimeh Janani[1] · Ali Reza Rezvani[2] ·
Gholam Hossein Grivani[1] · Ali Akbar Mirzaei[2]

Abstract A new hydrazone ligand, 4-methoxyacetophenone benzoyl hydrazone and its cobalt complex were synthesized and characterized using elemental analysis, Fourier transform infrared spectroscopy, ultraviolet–visible spectroscopy, ^{1}H NMR spectral data, and powder X-ray diffraction techniques. Moreover, the thermal gravimetric analysis and electrochemical (cyclic voltammetry) properties of the ligand and its complex were investigated. The catalytic ability of the Co-MABH complex as a new metal–organic catalyst in the Fischer–Tropsch reaction was investigated. The CO conversion under the operational conditions $T = 100$ °C, $P = 8$ atm and ratio of $H_2/CO = 2$ was found to be 50.21 %. The physicochemical characteristics of the catalyst were examined using scanning electron microscopy, and Brunauer–Emmett–Teller analysis at different operational stages.

Keywords Fischer–Tropsch synthesis · Heterogeneous catalysis · Hydrazone ligand · Impregnation

Introduction

The chemical characterization of hydrazones has been the focus of investigations in several areas of research due to the chelating capability of hydrazones and their potential applications [1–5]. These types of heterocyclic ligands form

✉ Ali Akbar Mirzaei
mirzaei@hamoon.usb.ac.ir

[1] School of Chemistry, Damghan University, Damghan, Iran

[2] Department of Chemistry, Faculty of Sciences, University of Sistan and Baluchestan,
Zahedan 98135-674, Iran

stable complexes with metal ions. Many of the complexes show excellent catalytic activity in different reactions at temperatures ≥100 °C [1]. Over the years, there have been many reports on their applications in homogeneous and heterogeneous catalysis [2–6].

This triggered us to study the synthesis of a novel hydrazone ligand derived from the condensation benzhydrazide and 4-methoxyacetophenone in the presence of concentrated HCl and its cobalt complex for Fischer–Tropsch synthesis (FTS). Various modes of coordination of the hydrazone ligand, MABH, are shown in Scheme 1. To date, a wide variety of hydrazone Schiff base complexes have gained recognition as catalysts for different reactions [1, 2], but the roles of these types of
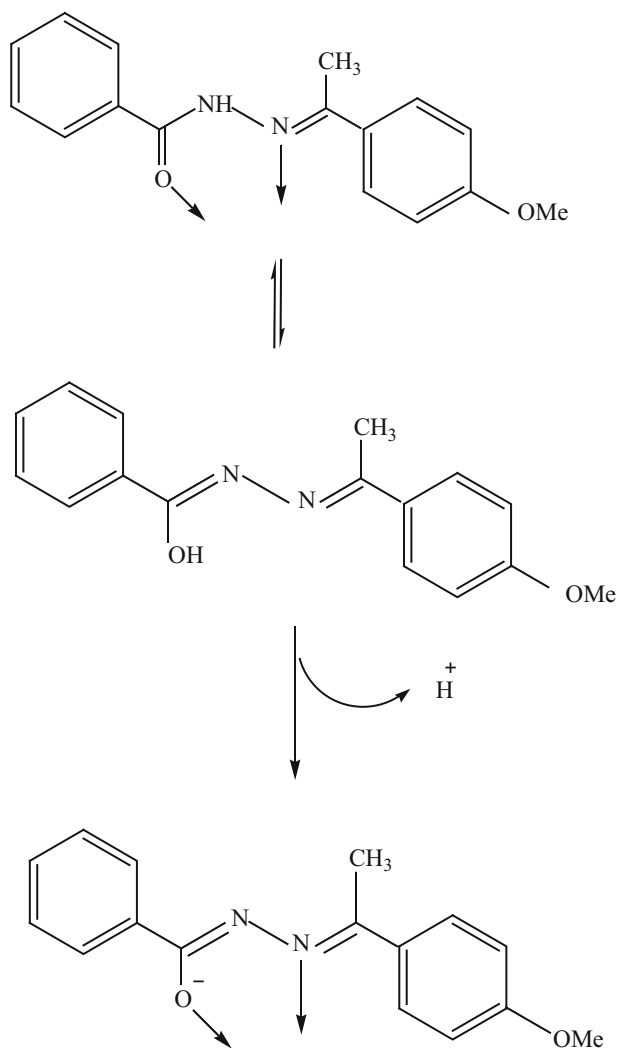
Scheme 1 Various modes of coordination of the hydrazone ligand [C$_6$H$_5$(CO)NHN=C(CH$_3$)C$_6$H$_4$OCH$_3$ (MABH)]

compounds as catalyst precursors for Fischer–Tropsch synthesis have not been explored. In the present study, we specifically designed and characterized a novel metal–organic catalyst derived from a cobalt hydrazone complex for FTS as an important process in the present-day transformation of coal, natural gas, or biomass into synthetic fuel. Research toward the development of new catalysts for the existing process remains a priority. However, the emphasis is shifting toward environmentally friendly, economically viable processes. In view of this, we are reporting the synthesis of new cobalt hydrazone complex as a novel heterogeneous catalyst for the first time for FTS application. Our new synthesized catalyst was named Co/γ-Al$_2$O$_3$. The results were compared with nitrate based impregnated Co (N)/γ-Al$_2$O$_3$ catalyst as a reference catalyst. So far, various catalysts have been studied for FTS reaction such as cobalt, iron and nickel based catalysts. Among these, the catalysts prepared from metal nitrate salts, are widely used for FTS reaction. However, in this study, the catalyst with cobalt nitrate (reference catalyst) was considered as a common FTS catalyst and the catalytic performance results were compared with new catalyst (cobalt hydrazone). In fact, an alternative strategy to modify the properties of supported catalysts is by choice of the starting metal complex. To further investigate the specific properties (such as selectivity and activity) of the FTS catalysts, we have chosen to investigate the effect of metal source on the reaction by preparing a novel and a common FTS catalyst.

Experimental

Materials and methods

Benzhydrazide, 4-methoxyacetophenone and cobalt nitrate hexahydrate (Merck KGaA, Germany) were used as received without further purification. All the solvents were reagent grade.

Fourier transform infrared (FT-IR) spectra were recorded using a Perkin-Elmer (USA) FT-IR spectrometer using KBr pellets.

Elemental analyses were performed on a Perkin-Elmer 2400 CHN S/O type analyzer. Thermogravimetric behaviors were recorded under air using the BAHR-STA 503 (Germany) thermal analyzer and electronic spectra, using a JASCO 7850 spectrophotometer (Kyoto, Japan).

X-ray powder analyses were conducted using a D8-ADVANCE Bruker (Germany) diffractometer operated at 35 kV and 30 mA generator using a Cu K$_\alpha$ line at 1.5460 Å as the radiation source.

Cyclic voltammograms of the ligand and the complex were recorded using a SAMA500 Electro Analyzer (MO, USA). This system consisted of three electrodes: a Pt disk working electrode (RDE), a Pt wire auxiliary electrode, and a reference saturated calomel electrode (SCE). The supporting electrolyte, 0.1 M tetrabutyl ammonium hexaflourophosphate (TBAH), was recrystallized two times from ethanol–water (1:1) and vacuum-dried at 110 °C overnight. The solutions were deoxygenated by bubbling with Ar for 15 min. Acetonitrile was distilled over alumina and degassed under vacuum before use in cyclic voltammetry.

The BET surface area of the catalyst (before and after the test) was measured by N_2 physisorption using a Quanachrome Nova 2000 automated system (USA). The catalyst was degassed under nitrogen atmosphere at 250 °C for 3 h. To obtain the BET surface area, the samples were evacuated at −196 °C for 66 min.

The morphology of the catalyst was observed using Cambridge S-360 (England) scanning electron microscope operating at 20 kV. The samples were coated with gold/palladium for 80 s in 20 s intervals before the measurements to avoid charging problems.

Preparation procedures

### Preparation of hydrazone ligand $C_6H_5(CO)NHN=C(CH_3)C_6H_4OCH_3$ (MABH)

A solution of 4-methoxyacetophenone (40 mmol = 6 g) methanol (40 mL) was heated for 10 min in presence of few drops of concentrated HCl. To this solution, a hot solution of benzhydrazide (40 mmol = 5.44 g) in methanol (30 mL) was added drop wise with constant stirring. The yellow product was heated under reflux for 2 h and then allowed to cool. After a few days, crystals of ligand were separated out and characterized by analytical and different spectral analysis methods. (see Fig. 1). Yield 86 %, Analytically Calculated for $C_{16}H_{16}N_2O_2$: C; 71.64 %, H; 5.97 %, N; 10.44 %, Found: C; 71.44 %, H; 6.07 %, N; 10.41 %.

Preparation of complex [Co(MABH)(NO₃)₂(H₂O)₂]

To an ethanolic solution (30 mL) of $Co(NO_3)_2 \cdot 6H_2O$ (2.91 g, 10 mmol), a hot ethanolic solution of hydrazone MABH (2.68 g, 10 mmol) was added with constant stirring. The solution was stirred at room temperature for 3 h and then kept in a refrigerator. Crystals appeared after 7 days (Fig. 2). Yield 78 %, Analytically Calculated for $CoC_{16}H_{20}N_4O_{10}$: C; 39.42 %, H; 4.10 %, N; 11.49 %, Found: C; 39.85 %, H; 4.56 %, N; 11.38 %.
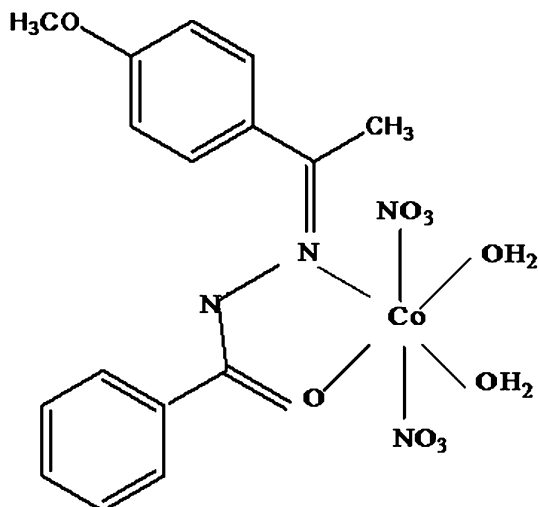
Catalyst preparation

Ethanol as solvent was dried and distilled under nitrogen before use. The complex was impregnated into γ-Al₂O₃ (dried in air at 750 °C for 5 h in order to
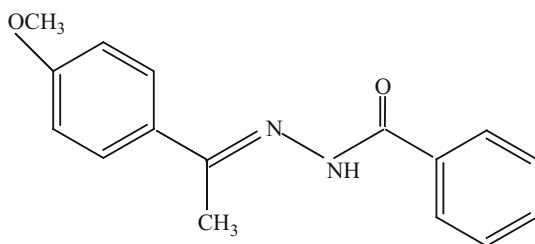
Fig. 1 Proposed structure of ligand [$C_6H_5(CO)NHN=C(CH_3)C_6H_4OCH_3$ (MABH)]

Fig. 2 Proposed structure of complex [Co(MABH)(NO$_3$)$_2$ (H$_2$O)$_2$]

dehydroxylate the surface) in nitrogenated ethanol under deoxygenated atmosphere (on a Schlenk line using standard air free methods). The catalyst was dried slowly under vacuum at room temperature for 10 h.

The catalyst with cobalt nitrate as a reference catalyst was also prepared for comparison purposes by impregnation of γ-Al$_2$O$_3$ and named as Co(N)/γ-Al$_2$O$_3$.

Catalytic evaluation

The FTS reaction was performed in a tubular stainless steel micro–fixed bed reactor. Schematic representation of the experimental set-up can be found in one of our previous papers [7].

Before testing, the catalyst was reduced with hydrogen at 80 °C for 5 h (H$_2$ flow rate = 60 mL/min) and then fed with the synthesis gas. The reactions were performed at T = 100 °C, P = 8 atm and ratio of H$_2$/CO = 2. In each test, 1.0 g catalyst was loaded and the reactor operated for ∼12 h to ensure that steady-state operation was attained. The catalytic performance results are given in terms of the CO conversion (%) calculated according to the normalization method:

$$CO\ conversion\ (\%) = \frac{(Moles\ of\ CO_{in}) - (Moles\ of\ CO_{out})}{Moles\ of\ CO_{in}} \times 100$$

The selectivity (%) toward the individual components on carbon- basis is calculated according to the same principle:

$$Selectivity\ of\ j\ product\ (\%) = \frac{Moles\ of\ carbon\ in\ product\ j}{Moles\ of\ converted\ CO} \times 100$$

Results and discussions

FT-IR spectral studies

The FT-IR spectrum of the complex was analyzed in comparison with that of the free ligand, MABH, in the region 4000–400 cm^{-1} (Figs. 3 and 4). The FT-IR spectrum of the ligand exhibits a strong band at 3183 cm^{-1}, which is assigned to the NH vibration. The bands centered at 1654 cm^{-1} and appearing around 1590 cm^{-1} are assigned, respectively, to υ(C=O) and υ(C=N) of the hydrazone [8]. For complex, the N–H absorption band appears at 3055 cm^{-1}, whereas the C=O band appears at 1603 cm^{-1}. Both of these bands indicate that, in this case, the ligand coordinated the metal in its keto form. Hydrazones such as those synthesized in this work may exist in the keto or in the enol tautomeric form in the solid state. The observation of strong C=O absorption bands around 1654 cm^{-1} in the infrared spectrum of the ligand suggests that the ligand is in the keto form in the solid state [9–11]. The tautomeric keto forms of the compound were also indicated by ^{1}HNMR spectroscopy, since OH signals of the enol form of the ligand were not observed, while the amide NH signals of the keto form appeared around 10.67 ppm. The infrared spectrum of the complex displays an IR absorption band at 1543 cm^{-1}, which can be assigned to the C=N stretching frequency of the coordinated ligand; whereas, for the free molecule, the same band is observed at 1590 cm^{-1} [12]. The shift of this band on complexation toward the lower wave number indicates coordination of the azomethine nitrogen to the metal center [13]. Further proof of the complexation for azomethine nitrogen is obtained from the appearance of a new band at 490 cm^{-1}, which is assignable to the Co–N stretching vibrations for
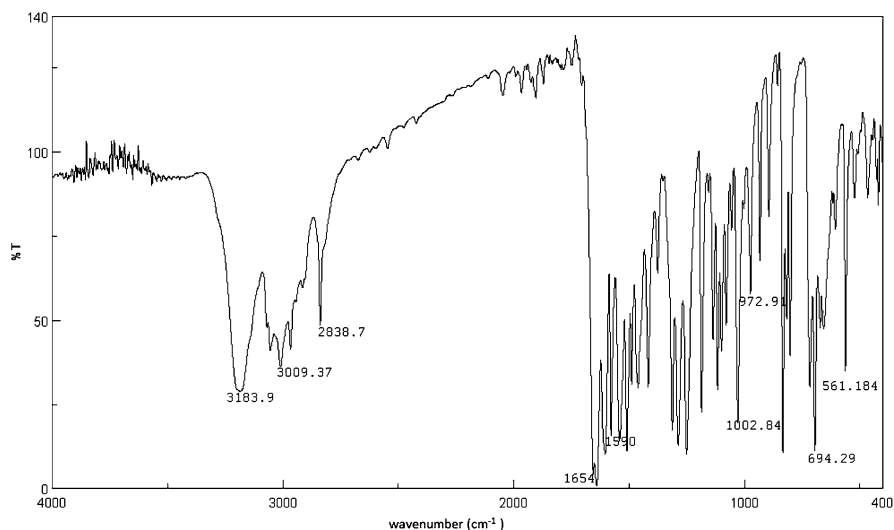
Fig. 3 FT-IR spectrum of ligand [C$_6$H$_5$(CO)NHN = C(CH$_3$)C$_6$H$_4$OCH$_3$ (MABH)] (400–4000 cm^{-1}): υ(NH) 3183 cm^{-1}, υ(C=O) 1654 cm^{-1}, υ(C=N) 1590 cm^{-1}, υ(N–N) 1002 cm^{-1}
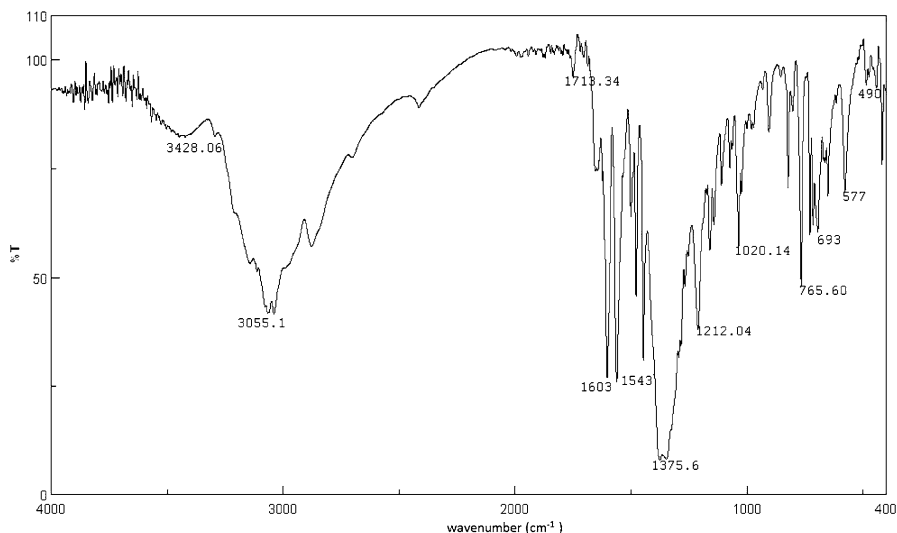
Fig. 4 FT-IR spectrum of complex [Co(MABH)(NO$_3$)$_2$(H$_2$O)$_2$] (400–4000 cm^{-1}): υ(NH) 3055 cm^{-1}, υ(C=O) 1603 cm^{-1}, υ(C=N) 1543 cm^{-1}, υ(N–N) 1020 cm^{-1}

complex [14]. The increase in N–N stretching frequency in the spectrum of the complex from 1002 to 1020 cm^{-1}, is due to the increase in the double bond character offsetting the loss of electron density via donation to metal and is a further confirmation of coordination of the ligand through the azomethine atom. In the FT-IR spectrum of the complex, bands of coordinated water ligands are observed at 3428 cm^{-1}. The band observed at 1713 cm^{-1} suggests the monodentate coordination of the nitrate group [15].

H NMR data for the ligand

The ^{1}H NMR spectrum of MABH in DMSO-d$_6$ shows three singlets corresponding to –NH, –OCH$_3$ and –CH$_3$ (see Fig. 5). The singlet at $\delta = 10.67$ ppm represent –NH. The peak at $\delta = 3.79$ ppm is assigned to –OCH$_3$. Another singlet at $\delta = 2.32$ ppm which represents the aliphatic CH$_3$. The aromatic protons appear as multiplets at 6.98–7.87 ppm. (500 MHz, DMSO).

Electronic spectra

The electronic spectra for the hydrazone ligand and the complex recorded in ethanol. The electronic spectral data of the ligand exhibit two bands in the UV region. The band appearing at 222 nm is attributed to intraligand of $\pi \rightarrow \pi^*$ transition. The other band observed at 304 nm can be assigned to n $\rightarrow \pi^*$ electronic transition (Fig. 6). The loss of the absorption band at 304 nm in the presence of a few drops of HNO$_3$ indicated this band is assigned to n $\rightarrow \pi^*$ transition [2, 16]. There is a slight shift in these bands during complexation ($\pi \rightarrow \pi^*$ at 246 nm and
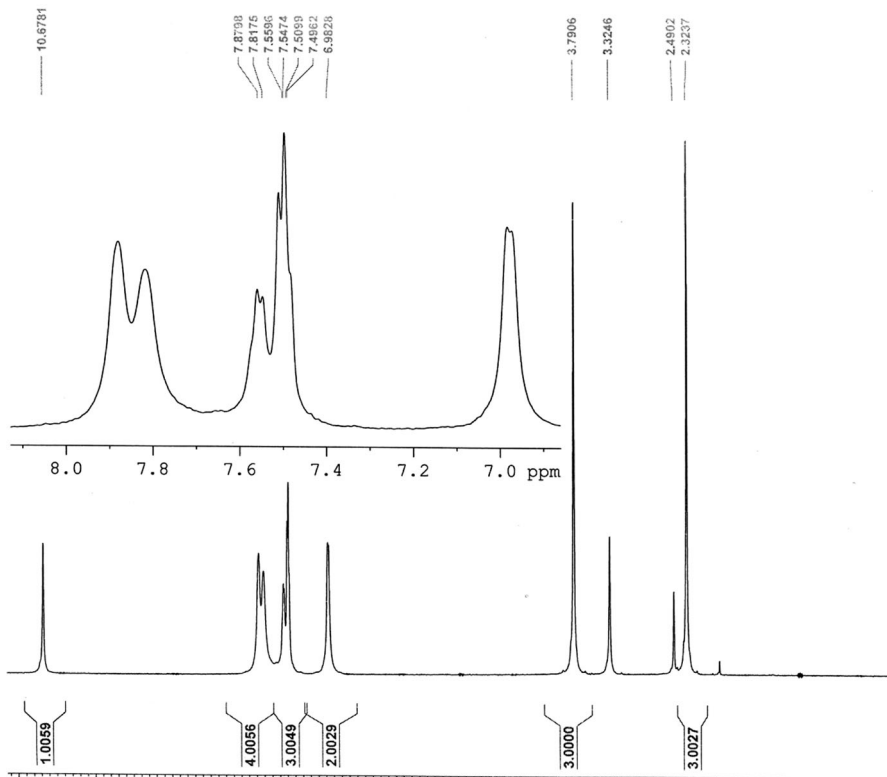
Fig. 5 ^{1}H NMR spectrum of ligand $[C_6H_5(CO)NHN=C(CH_3)C_6H_4OCH_3$ (MABH)] in deuterated DMSO (DMSO-d_6) at 500 MHz, δ (ppm): 10.67 (s, –NH), 3.79 (s, –OCH$_3$), 2.32 (s, CH$_3$)
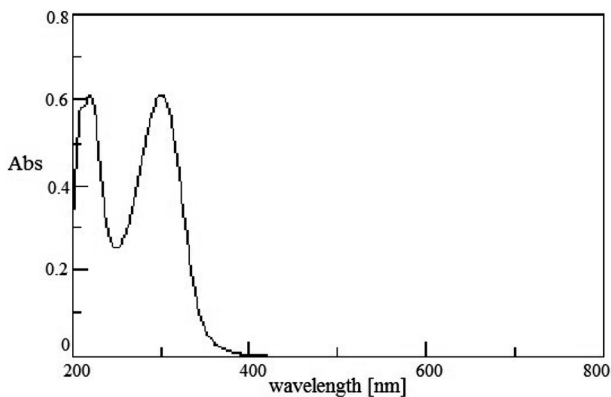
Fig. 6 UV-Visible spectrum of ligand $[C_6H_5(CO)NHN=C(CH_3)C_6H_4OCH_3$ (MABH)] in ethanol (10^{-5} M, 200–800 nm), λ = 222 nm (π → π*), 304 nm (n → π*)

n → π* at 310 nm) [17]. Ethanolic solution of the complex has been used to record the UV–Vis spectrum of complex. In the spectrum of the complex, the band of the azomethine chromophore n → π* transition is shifted to lower frequencies, which means that the imine nitrogen atom is involved in coordination to the metal ion [18]. The electronic spectrum of the cobalt(II) complex displayed bands at 680 and 610 nm. These two bands are assignable to $^4T_{1g}(F) \rightarrow {}^4A_{2g}(F)$ (υ_2) and $^4T_{1g}(F) \rightarrow {}^4T_{2g}(P)$ (υ_3) transitions, respectively, in an octahedral environment [19]. The lowest band υ_1, could not be seen because of the restricted range of the instrument used. Moreover, the spectrum shows one intense band at 322 nm could be assigned to the charge-transfer band [20].

Electrochemical studies

The cyclic voltammograms of the ligand and its cobalt complex in DMF are shown in Figs. 7 and 8, which show ligand-based reductions at −0.76 V (quasireversible reduction of the aroyl hydrazone moiety) and −1.2 V (azomethine (C=N) reduction), respectively [12]. Voltammogram of the complex showed a peak at −0.14 V (versus SCE) which could be attributed to the reduction of Co(III) to Co(II). Another peak, at −0.12 V (versus SCE), was attributed to the oxidation of Co(II) to Co(III). This process is thus reversible, characterized by a peak-to-peak separation (ΔE_p) of 20 mV that remains unchanged upon varying the scan rate. The anodic peak current (i_{pa}) was almost equal to the cathodic peak current (i_{pc}), as expected for a reversible electron transfer process [14].
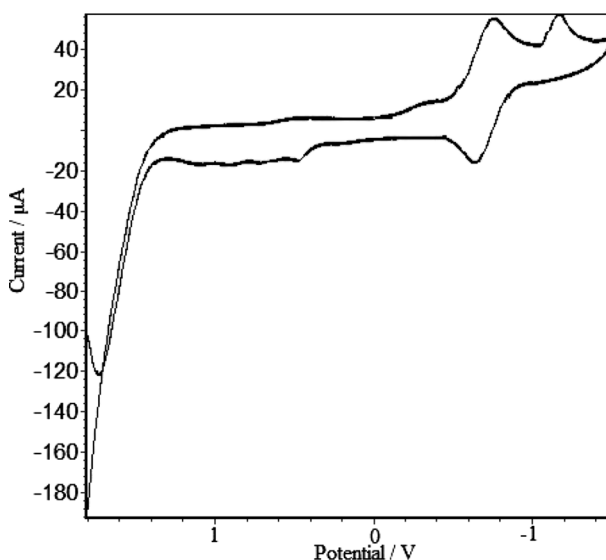
Fig. 7 Cyclic voltammogram of ligand [$C_6H_5(CO)NHN=C(CH_3)C_6H_4OCH_3$ (MABH)] in DMF (The supporting electrolyte, 0.1 M tetrabutyl ammonium hexaflourophosphate (TBAH), scan rate: 500 mVs^{-1}, T = 25 °C), ligand-based reductions at −0.76 V (quasireversible reduction of the aroyl hydrazone moiety) and −1.2 V (azomethine (C = N) reduction)
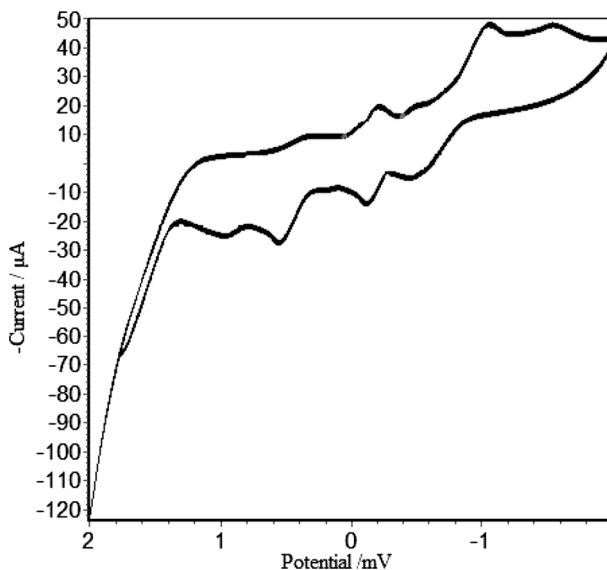
Fig. 8 Cyclic voltammogram of complex $[Co(MABH)(NO_3)_2(H_2O)_2]$ in DMF (The supporting electrolyte, 0.1 M tetrabutyl ammonium hexaflourophosphate (TBAH), scan rate: 500 mV s^{-1}, T = 25 °C), the peak at −0.14 V (versus SCE), which could be attributed to the reduction of Co(III) to Co(II). Another peak, at −0.12 V (versus SCE), was attributed to the oxidation of Co(II) to Co(III)

Thermogravimetric studies

TG and DTA studies were carried out on the ligand and its complex in the 25–800 °C temperature range. The thermal analyses showed that there were two endothermic peaks in the DTA curve of the ligand. The first appeared at 180 °C can be attributed to the melting point of the ligand, because no loss of weight was observed in the TG curve. The second peak appeared above 270 °C, indicating decomposition of the ligand, which was complete at about 350 °C.

The thermal decomposition curve of the complex differed from that of the ligand. The first step in the decomposition sequence at 110–145 °C corresponded to the loss of the water molecules present in the complex, which was in agreement with the calculated value (Calculated: 7.39 %, Found: 7.44 %). The second step in the decomposition of the complex started from about 300 °C and continued up to 450 °C, as shown by the horizontal plateau on the TG curve, indicating the decomposition of the organic part of the chelate in the last step, which left metal oxide residues at the final temperature (Calculated: 86.91 %, Found: 85.7 %). The final weight of the residue corresponded to the metal oxides (Fig. 9). The decomposition temperature of the complex was higher than that of the ligand, indicating that the thermal stability of the complex increased due to the ligand coordinating with metal ions to form a stable ring.
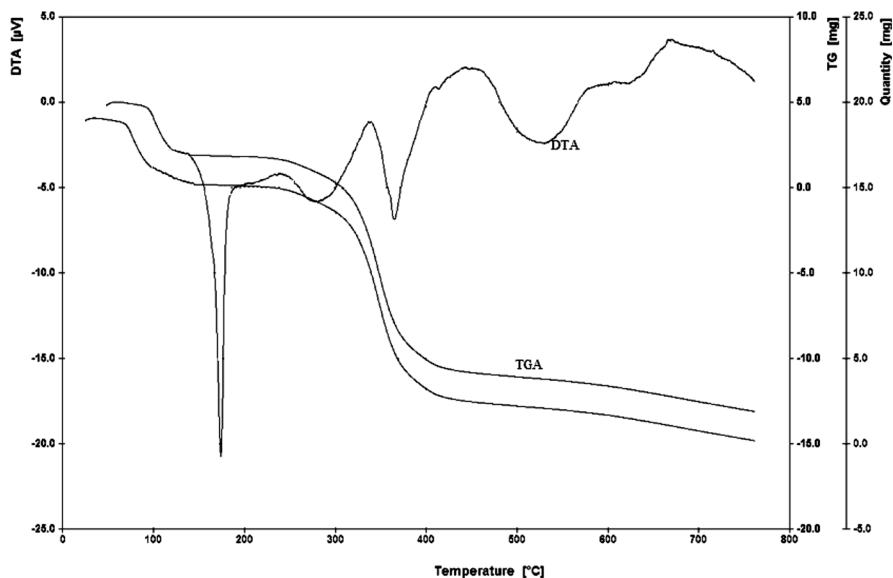
Fig. 9 Thermoanalytical curves (TGA/DTA) of complex [Co(MABH)(NO$_3$)$_2$(H$_2$O)$_2$] (Temperature range: 25–800 °C), The first step in the decomposition sequence at 110–145 °C corresponded to the loss of the water molecules present in the complex and the second step in the decomposition of the complex started from about 300 °C and continued up to 450 °C, as shown by the horizontal plateau on the TG curve, indicating the decomposition of the organic part of the chelate in the last step, which left metal oxide residues at the final temperature

X-ray powder diffraction

The X-ray diffraction pattern of the complex records 20 reflections between 10° and 80° (2θ), with maxima at 2θ = 21.44°, corresponding to a value of d = 4.1 Å (Table 1). The main peaks of the complex have been indexed using computer software by a trial and error method [21]. The characteristics of several symmetry systems were monitored until a good fit could be obtained between the observed and calculated 2θ and sin^{2}θ values. The method also yields h, l, k values (Miller indices). Comparison of values of 2θ and sin^{2}θ indicates good agreement between the calculated and observed values; 2θ and sin^{2}θ, based on the assumption of a monoclinic structure [22]. The small difference in the observed d spacing could be due to a difference in unit cell dimensions. The structure of the complex yields values for the lattice constant of $a = 7.21$ Å, $b = 12.38$ Å, $c = 33.13$ Å, $\alpha = 90°$, $\beta = 94°$, $\gamma = 90°$ and unit cell volume V = 2949 Å^3. In addition to these lattice parameters, the conditions such as $a \neq b \neq c$ and $\alpha = \gamma = 90°$, $\beta \neq 90°$ required for the sample to be monoclinic was tested and found to be satisfactory.

Catalytic performance studies

The catalytic activity of the hydrazone cobalt complex was investigated for the FTS. The catalytic performance results of the samples are presented in Table 2. The F-T

Table 1 X-ray diffraction data of complex

d(Å)	Rel Int%	Observed $\sin^2\theta$	Calculated $\sin^2\theta$	hkl	Observed 2θ	Calculated 2θ
4.1	100.00	0.0351	0.0349	0,0,8	21.44	21.53
4.8	57.93	0.0259	0.0257	1,1,4	18.40	18.39
4.4	48.32	0.0306	0.0306	1,1,5	20.03	20.06
3.0	25.34	0.0631	0.0655	0,4,1	29.05	29.40
3.8	23.86	0.0405	0.0408	1,0,7	23.02	23.20
1.9	18.96	0.1602	0.1640	2,4,5	46.91	46.46
2.0	16.61	0.1393	0.1480	3,1,5	43.60	44.10
5.2	15.84	0.0213	0.0219	1,1,3	16.78	16.97
3.1	12.53	0.0586	0.0615	2,0,4	27.88	28.40
2.2	11.97	0.1209	0.1220	2,4,4	40.40	40.12
2.3	9.83	0.1092	0.1110	−2,4,1	38.31	38.38
3.5	8.76	0.0475	0.0484	−1,3,2	25.22	25.22
1.8	6.93	0.1812	0.1821	3,2,1	50.20	49.04
5.5	6.29	0.0191	0.0197	−1,1,3	15.91	16.05
3.6	6.02	0.0443	0.0453	0,3,4	24.14	24.50
5.7	5.15	0.0179	0.0182	0,2,2	15.32	15.52
3.4	4.75	0.0508	0.0510	2,1,1	26.06	25.96

Table 2 Catalytic performance of the samples for F-T synthesis

Samples	CH_4selectivity%	C_2H_6	C_2H_4	C_3H_8	C_3H_6	C_4H_{10}	C_4H_8	C_5^+
Co/γ-Al$_2$O$_3$	13.07	14.10	17.10	8.09	17.20	8.23	14.12	8.02
Co(N)/γ-Al$_2$O$_3$	33.01	11.42	6.12	5.31	10.64	2.68	9.36	3.68

reaction was performed in a tubular stainless steel micro–fixed bed reactor. Prior to the testing, the catalyst was reduced with pure hydrogen at 80 °C for 5 h, and then fed with the synthesis gas. The operational reaction conditions were 100 °C, 8 atm and ratio of $H_2/CO = 2$. The catalyst (1 g) was loaded into the reactor. Then, the reactor was pressurized to the desired reaction pressure, and gradually changed to syngas to prevent overhead by the fresh catalyst. Performance of the cobalt nitrate catalyst was also investigated as a reference catalyst. The obtained results showed that it was poorer than that with cobalt hydrazone complex as a precursor, possibly because the cobalt nitrate was small and unfavorable for dissociation and adsorption of CO over the catalyst with complex as a precursor.

The most important observation from the current study can be summarized as below:

The cobalt hydrazone catalyst shows a higher selectivity towards light olefins, and it produces less methane (13.07 %) compared with cobalt nitrate catalysts (33.01 %) (Table 2). Furthermore, the activity of the new catalyst was investigated at different temperature (T = 100, 200, 300 °C, P = 5–8 atm) and it was found that the activity of the new catalyst depends on the temperature and pressure reaction,

i.e, with a decrease in the temperature and increase in the pressure, activity increases. The decrease in activity could be because cobalt shows a tendency to sinter the support at high temperature. This feature is important to the industrial processes of FTS, as a lower temperature results in fewer amounts of coke (CO to C conversion) precipitated on the surface of the catalyst. Coke formation on the catalyst surface may cause catalyst deactivation.

The broad absorption band at 3443 cm^{-1} in the FT-IR spectrum of the catalyst is assigned to OH stretching vibration of physically adsorbed water. The H-OH bending vibrations of the adsorbed water appear at about 1634 cm^{-1} in the catalyst.

The BET results of the catalyst tested at $H_2/CO = 2/1$ that compare the samples before and after the test are presented in Table 3. The catalyst has a higher specific area (104 m^2/g) before the test, than the specific area of the catalyst after the test (100.4 m^2/g). Upon impregnation of both catalysts onto the support (alumina), the surface area decreased, especially in new catalyst which indicated additional pore blockage by cobalt hydrazone complex. To a greater extent, the surface area may be increased by decreasing the mean pore width value of the catalyst. Indeed it may easily be shown that the surface area S is related to the pore volume V_p and pore radius r_p in a model with cylindrical monomodal pores by expression [23]:

Table 3 BET results of precursor and catalyst (before and after the test)

Specific surface area (m^2/g)		
Precursor	Fresh catalyst	Used catalyst
112.10	104	100.4
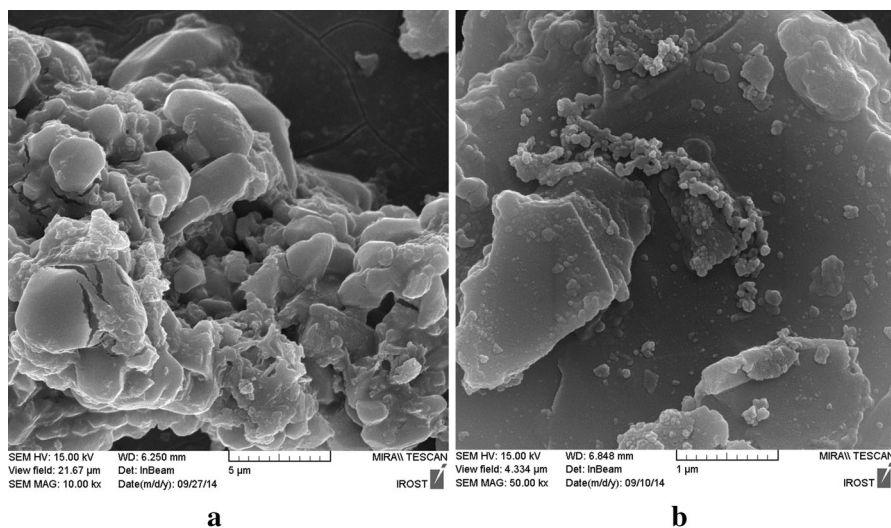
Fig. 10 SEM images of catalyst Co/γ-Al$_2$O$_3$ **a** before the test, **b** after the test (The operational reaction conditions: T = 100 °C, P = 8 atm and $H_2/CO = 2$)

$$S = 2V_p / r_p$$

Therefore the smaller the pore volume leads to the smaller the surface area.

The morphological properties of the catalyst (pre- and post-test) were characterized using scanning electron microscopy (SEM). The obtained SEM micrographs are presented in Fig. 10 and show differences in the morphology of the pre- and post-test catalyst. The electron micrographs obtained from freshly catalyst depicts several irregularly–shaped particles of different sizes that form a highly dense agglomeration (Fig. 10a). After the FTS reaction, the morphological characteristics of the used catalyst is completely different (Fig. 10b) and this tested sample is comprised of particles of different sizes that agglomerate together and make a more sticky texture than seen in the fresh sample, this may be due to a sintering phenomenon after the test [24, 25]. These results are in agreement with the BET results, which showed that the specific surface area is smaller for the used catalyst than for the freshly catalyst. The high specific surface area of catalyst before the test allows a high degree of metal dispersion.

Conclusion

A new hydrazone ligand and its cobalt complex has been synthesized and characterized using various spectroscopic and nonspectroscopic methods. According to the analytical and spectral data, the complex is formed by the coordination of N, O atoms of ligand and the hydrazone ligand is in the keto form. The experimental and simulated XRD pattern of the complex is in agreement with each other, verifying the phase purity of product. The catalytic activity of the complex has been examined for hydrogenation of carbon monoxide (FTS). The complex was loaded on γ-Al$_2$O$_3$. BET surface area measurements show that the precursor has a higher specific area than the catalyst and these results are in agreement with SEM results. Its FTS catalytic activity was evaluated in a tubular stainless steel micro–fixed bed reactor (100 °C, 8 atm, 2H$_2$:1CO). It was a specific example that a hydrazone metal complex was used as a catalyst precursor toward hydrogenation of CO reaction for synthesis of clean fuels.

References

1. İspir E (2009) Dyes Pigments 82:13–19
2. Pouralimardan O, Chamayou AC, Janaik C (2007) Hosseini monfared H. Inorg Chim Acta 360:1599–1608
3. Gupta KC, Sutar AK, Lin CC (2009) Coord Chem Rev 253:1926–1946
4. Biswas C, Chattopadhyay SH, Drew MGB, Gosh A (2007) Polyhedron 26:4411–4418
5. Kuriakose M, Kurup MRP, Suresh E (2007) Polyhedron 26:2713–2718
6. Tu-Lin C, Quan-Chang G, Jain-She Z, Gai Z (2008) Chin J Chem 26:1079–1084

7. Arsalanfar M, Mirzaei AA, Atashi H, Bozorgzadeh HR, Vahid S, Zare A (2012) Fuel Process Technol 96:150–159
8. Srinivasan S, Annaraj J, Athappan PR (2005) J Inorg Biochem 99:876–882
9. Calinescu M, Emandi A, Şerban I, Pop V (2003) Synth React Inorg Met-Org Chem 33:1927
10. Ainscough EW, Brodie AM, Denny WA, Finlay GJ, Gothe SA, Ranford JD (1999) J Inorg Biochem 77:125
11. Lee PF, Yong CT, Fon D, Vittal JJ, Ranford JD (2003) Polyhedron 22:2781
12. Addison A.W, Rao T.N, Reedijk J, van Rijn J, Verschoor G.C (1984) J Chem Soc Dalton Trans 1349
13. Conley RT (1966) Infrared spectroscopy. Allyn & Bacon, Boston
14. Banerjee S, Ray A, Sen S, Mitra S, Hughes DL, Butcher RJ, Batten SR, Turner DR (2008) Inorg Chim 361:2692–2700
15. Gerloch M, Mason R (1965) J Chem Soc 52:296
16. Gup R, Kürkan B (2005) Spectrochim Acta, Part A 62:1188–1195
17. Sreeja PB, Kurup MRP, Kishore A, Jasmin C (2004) Polyhedron 23:575–581
18. Nakamoto K (1997) Infrared and raman spectra of inorganic and coordination compounds, Part: B, 5th edn. Wiley, New York, p 23
19. Underhill AE, Billing DE (1966) Nature 210(5038):834–835
20. Viñuelas-Zahínos E, Maldonado-Rogado MA, Luna-Giles F, Barros-García FJ (2008) Polyhedron 27:879–886
21. Cullity BD (1977) Elements of X-ray diffraction, 2nd edn. Addison-Wesley, Reading
22. Mullica DF, Sappenfield EL, Perkins HO (1989) J. Solid State Chem 78:301–306
23. Perego C, Villa P (1997) Catal Today 34:281–305
24. Janani H, Rezvani AR, Grivani GH, Mirzaei AA (2015) J Inorg Organomet Polym Mater 54:1–14
25. Galarraga, C.E (1999) Heterogeneous Catalyst for the Synthesis of Middle Distillate Hydrocarbons, University of Western Ontario, M.S.c Thesis, London